

## **A modelling-based assessment of the imprint of storms on wind waves in the western Mediterranean Sea**

Toomey, Tim; Sayol Espana, Juanma; Marcos, Marta; Jorda, Gabriel ; Campins, Joan

**DOI**

[10.1002/joc.5849](https://doi.org/10.1002/joc.5849)

**Publication date**

2018

**Document Version**

Accepted author manuscript

**Published in**

International Journal of Climatology

**Citation (APA)**

Toomey, T., Sayol Espana, J., Marcos, M., Jorda, G., & Campins, J. (2018). A modelling-based assessment of the imprint of storms on wind waves in the western Mediterranean Sea. *International Journal of Climatology*, 39(2), 878-886. <https://doi.org/10.1002/joc.5849>

**Important note**

To cite this publication, please use the final published version (if applicable).  
Please check the document version above.

**Copyright**

Other than for strictly personal use, it is not permitted to download, forward or distribute the text or part of it, without the consent of the author(s) and/or copyright holder(s), unless the work is under an open content license such as Creative Commons.

**Takedown policy**

Please contact us and provide details if you believe this document breaches copyrights.  
We will remove access to the work immediately and investigate your claim.

1 **A modeling-based assessment of the imprint of storms on**  
2 **wind waves in the Western Mediterranean Sea**

3 **T. Toomey\*<sup>1</sup> , J.M. Sayol<sup>2</sup> , M. Marcos<sup>3,4</sup> , G. Jordà<sup>3,4</sup> , J. Campins<sup>5</sup>**

4 <sup>1</sup>ENSTA-Bretagne, Department STIC-HOP, Brest, France

5 <sup>2</sup>Delft University of Technology, Department of Hydraulic Engineering, Delft, The Netherlands

6 <sup>3</sup>Department of Physics, University of the Balearic Islands, Palma, Spain

7 <sup>4</sup>IMEDEA (UIB-CSIC), Esporles, Spain

8 <sup>5</sup>Agencia Estatal de Meteorología (AEMET), Palma de Mallorca, Spain  
9

10  
11 **Keywords:**

12 Western Mediterranean Sea, atmospheric cyclones, wind-wave climate, wind climate  
13  
14  
15  
16  
17

---

18 \*Corresponding author: T. Toomey, [tim.toomey@ensta-bretagne.org](mailto:tim.toomey@ensta-bretagne.org)

19 [tim.otuma@gmail.com](mailto:tim.otuma@gmail.com)  
20

---

## 21 **Abstract**

22 This study analyzes the distribution of ocean wind waves in response to extra-tropical  
23 cyclones over the Western Mediterranean Sea. To this end we use an ERA40-based database of  
24 atmospheric cyclones and a 3-hourly wind wave hindcast with high horizontal resolution ( $\frac{1}{6}^\circ$ ) based on an ERA40 downscaled forcing for the region of study. The imprint of winds  
25 on surface waves is evaluated through composites of modeled significant wave height, surface  
26 wind and wave peak period collocated under the storms. Results highlight an asymmetric  
27 pattern that depends on the translational speed and size of the cyclonic perturbations.  
28 Uncertainties of the composites are at most 10% at 95% confidence interval, with an average  
29 maximum perturbation of significant wave height near 2 m for those cyclones moving faster  
30 than 10 m/s.  
31

## 32 **1 Introduction**

33 In recent years a great effort has been dedicated to better understand the formation and  
34 propagation of ocean surface waves under the presence of atmospheric cyclones. Due to the  
35 major threat that they represent, there have been historically many works focused on tropical  
36 cyclones (TCs) (see e.g. Cline, 1920; Tannehill, 1936; Wright *et al.*, 2001; Moon *et al.*, 2003,  
37 2004; Fan *et al.*, 2009; Doyle *et al.*, 2012; Holthuijsen *et al.*, 2012; Stephens and Ramsay, 2014;  
38 Timmermans *et al.*, 2017). Conversely, less attention has been paid to extra-tropical cyclones,  
39 being most of the works focused on particular events occurring in North and South Atlantic  
40 Ocean (see e.g. Cardone *et al.*, 1996; Innocentini and Neto, 1996; da Rocha *et al.*, 2004;  
41 Guimarães *et al.*, 2014). A good example of that is the Mediterranean Sea basin, with one of the  
42 highest rates of cyclogenesis in the world (Jansà, 1997; Sartini *et al.*, 2015). There, low-pressure  
43 perturbations develop quickly due to the interaction of the air with the mountains surrounding

44 the basin. Compared to TCs, these extra-tropical lows are weaker, smaller and shorter-living.  
45 Even so, their intense wind and torrential rain are enough to give rise to periodically harmful  
46 events with a huge amount of material loss and, occasionally, of human lives. Coastal floods by  
47 storm surges and strong beach erosion and damage on marine infrastructures by waves are  
48 recurrent during these events (see e.g. De Zolt *et al.*, 2006; Harley *et al.*, 2017).

49 This study focuses on the Western Mediterranean, where the formation of cyclones or  
50 the intensification of other low-pressure disturbances traveling from the Atlantic Ocean or North  
51 of Africa places that region as one of the most active of the Northern Hemisphere ([Jansà, 1997](#);  
52 [Campins et al., 2011](#)). The Mediterranean region favors a wide range of mechanisms as  
53 formation or deepening of mid-latitude perturbations by the orography and their fueling by low-  
54 level baroclinicity and/or low-level moisture sources (Trigo *et al.*, 2002). Origin, properties (e.g.  
55 size, structure and lifetime) and paths of cyclones in the Mediterranean Sea have been the  
56 subject of previous research (a complete review is presented in Lionello *et al.*, 2006). As a  
57 result, there are available databases of storms including their trajectory, center position and size  
58 (see e.g. Campins *et al.*, 2011; Dacre *et al.*, 2012).

59 Recently Besio *et al.* (2017) have discussed the spatial distribution of wave storms  
60 sequences in the Mediterranean Sea from a coastal hazard perspective using a wave hindcast.  
61 Alternatively, here we take advantage of the existence of simultaneous cyclone tracks and a high  
62 resolution wave hindcast to analyze the spatial distribution of ocean surface waves under  
63 atmospheric cyclones in the Western Mediterranean Sea. More in detail, we are interested in  
64 answering the following three questions: do these weaker extra-tropical cyclones leave a clear  
65 signature on ocean surface waves? How this pattern changes with cyclone properties (different  
66 size, translational velocity or direction of propagation)? How do their imprints compare to those  
67 of TCs? To respond to these questions we have performed composites of significant wave  
68 height, wave peak period and surface wind field collocated under atmospheric cyclones.

69           The article is organized as follows: Section 2 introduces the database of cyclones and  
70 the wave reanalysis; Section 3 describes the methodology followed to make the composites;  
71 Section 4 presents the composites of wave and wind fields for cyclones grouped by size and  
72 translational speed; finally, Section 5 discusses the results and outlines the main conclusions.

## 73   **2 Data**

74           A cyclone climatology for the Mediterranean Sea spanning the period 1958-2001 and  
75 based on ERA40 re-analysis mean sea level pressure data set has been used (Campins *et al.*,  
76 2011). It consists of 6-hourly positions, timing and radii (assuming a circle) of a total of 81762  
77 observations corresponding to 34612 different cyclones. The spatial resolution is  $1.125^\circ$  in both  
78 latitude and longitude ( $\approx 125$  km), derived using the tracking algorithm firstly presented by  
79 Picornell *et al.* (2001) and further developed in (Campins *et al.*, 2011). The robustness of this  
80 method has been confirmed by Lionello *et al.* (2016) through an inter-comparison of 14-cyclone  
81 detection and tracking methods using the ERA Interim reanalysis. Despite the different spatial  
82 resolution of ERA40 and ERA-Interim wind fields it is expected that the size and center of  
83 cyclones (and then the cyclonic wind fields) will be similar for the big moving cyclones here  
84 studied, with an average radii of 500 km.

85           To investigate the wave climate in the basin, a wind wave reanalysis over the Western  
86 Mediterranean Sea has been used. It has been generated using the WAM model (The Wamdi

87 Group, 1988), in a grid of  $\frac{1}{6}^\circ$  of spatial resolution fed with 10-m wind fields obtained from

88 ARPERA, a dynamical downscaling of ERA40 with a spatial resolution over the Mediterranean  
89 Sea of 40-50 km (Jordà *et al.*, 2012; Martínez-Asensio *et al.*, 2013). [The ARPERA hindcast  
90 simulation covers the period 1958–2001 and has been run using a global stretched-grid version  
91 of the ARPEGE-Climate model \(Déqué and Piedelievre, 1995; Déqué, 2007\). The ARPERA](#)

92 [dataset is temporally consistentcy over the entire period and provides realistic interannual](#)  
93 [variability \(nudging towards ERA40\). Moreover, its resolution of 50 km has been demonstrated](#)  
94 [to be enough to significantly improve the representation of the extremes over the sea \(Jordà et](#)  
95 [al 2012\).](#) Output fields consist of 3-hourly values of the wave parameters, namely significant  
96 wave height ( $H_s$ ), calibrated by Martínez-Asensio *et al.* (2013) on the basis of in-situ buoy  
97 observations, wave direction and wave peak period ( $T_p$ ). Wind-sea ( $H_s^{\text{wind-sea}}$ ) and swell ( $H_s^{\text{swell}}$ )  
98 components of significant wave height are also provided separately. The corresponding monthly  
99 mean field of each wave parameter at each grid point has been removed (except for  $T_p$ ), as we  
100 focus on the imprint of winds generated by cyclones on surface waves. Therefore, all the results  
101 presented hereinafter correspond to wave anomalies, unless otherwise stated.

### 102 **3 Methods**

103 To explore the impact of cyclones on the wave climate, we have selected those events  
104 whose center and at least 50% of their surface are located over the sea. This threshold has been  
105 chosen as a trade-off to ensure that the impact of cyclones occurs mostly over the sea surface  
106 and that the number of cyclones to be analyzed is large enough. Furthermore, we have kept the  
107 cyclones with a non-zero translational speed (TS). The TS has been calculated as the ratio  
108 between the distance and time at two consecutive time steps. This reduces the initial data set to  
109 5178 observations corresponding to 2537 different cyclones (see their spatial distribution in  
110 Figure S1).

111 As expected, most of the cyclones are located around the Gulf of Genoa (Figure S1),  
112 known to be an active region in terms of cyclogenesis in the Western Mediterranean (Jansà,  
113 1997; Trigo *et al.*, 1999; Maheras *et al.*, 2001; Nissen *et al.*, 2010; Campins *et al.*, 2011). The  
114 same pattern arises when intensity of cyclones (further defined in section 4.2) is mapped.  
115 Among all the observations considered, 35.59% of cyclones occur during the winter season. In  
116 addition, when only the strongest 10% events are concerned, almost half of them occur in winter

117 (45.71%) in agreement with earlier studies (Trigo *et al.*, 1999; Maheras *et al.*, 2001; Besio *et al.*,  
118 2017).

119 For each of the selected cyclones and at every time step, collocated wave fields are  
120 extracted over the sea area covered by the cyclone. We have kept all time steps for each  
121 cyclone, instead of that of maximum intensity, because in this region the intensity does not  
122 show large variations during the cyclone life time and because a reduced number of cases would  
123 diminish the statistical significance of the analyses. Therefore, unlike with large scale, intense  
124 extra-tropical storms (Rudeva and Gulev, 2007), we have considered that the imprint on waves  
125 is equally important during all cyclone stages. The wave fields associated to each individual  
126 cyclone have undergone a two-step transformation. Firstly, the wave fields are rotated so that  
127 the corresponding cyclone direction is set upwards. Secondly, the wave fields are normalized  
128 according to each cyclone radius. Normalized and rotated wave fields are then linearly  
129 interpolated onto a regular grid of  $301 \times 301$  points, so the resulting fields are comparable to  
130 each other, irrespective of the size of the cyclone. Composites are built by averaging normalized  
131 and rotated wave fields. Their uncertainties are calculated as the 95% confidence interval over  
132 the mean value (ME: Margin error), assuming a t-Student distribution. In addition to the wave  
133 parameters provided by the numerical simulation, the impact of the cyclones on the wave age  
134 (WA) has also been explored. ~~Finally, the relationship between the maximum Hs and maximum~~  
135 ~~wind speed has been quantified using an empirical polynomial formula.~~ Finally, the relationship  
136 between the maximum Hs and maximum wind speed has been quantified by fitting a  
137 polynomial function.

138 Despite the cyclone tracks database and the wave reanalysis have been generated from  
139 slightly different wind fields (~~the dynamical downscaling has smoothed somehow the wind~~  
140 ~~fields~~) it is expected that the cyclonic surface wind field matches reasonably well with the size  
141 and position of the cyclone. Figure 1 presents the tracking of one cyclone with the surface wind

142 field superimposed for successive time steps. Additionally, the composite of the wind field for  
143 all cyclones shown in Figure S2 confirms a good general agreement, except for a little  
144 displacement of the center, likely due to the different wind field spatial resolution. However this  
145 small deviation does not alter the conclusions of this work, as will be shown later.

## 146 **4 Results**

147 Composites of wave parameters have been calculated for different cyclone  
148 characteristics in order to explore and isolate their impact on the wave fields. These features  
149 include the translational speed of the cyclone (TS), its intensity and its size. Each case is  
150 described in detail in this section.

### 151 **4.1 Translational speed of cyclones**

152 Figure 2 shows the spatial distribution of Hs (total as well as wind-sea and swell  
153 components) under cyclones for three ranges of TS:  $< 5$  m/s, 5 to 10 m/s and  $> 10$  m/s. These  
154 values have been chosen to ensure a representative sample in each case (note that the number of  
155 cyclones is indicated in the figure). In all cases higher waves are found in the rear-right quadrant  
156 of the cyclone, where winds are stronger because the cyclone wind velocity adds up to the  
157 cyclone displacement (the opposite occurs for left quadrants). This is in agreement with the  
158 general rule that more intense winds and larger waves develop in the rear right quadrant (Cline,  
159 1920; Tannehill, 1936).

160 | As the TS increases, wind speed anomalies (~~S~~) increases together with Hs and the  
161 corresponding zones in the rear-right quadrant become more localized. Also the overall left-  
162 right asymmetry becomes more evident with higher TS. The uncertainties, plotted as dark  
163 purple lines, reach no more than 10% of Hs inside cyclones (green circle), indicating thus that  
164 the results are significant.



165           The spatial distribution of  $H_s^{\text{wind-sea}}$  (Figure 2, middle row) mimics to a large extent that  
166 of  $H_s$ . Since  $H_s^{\text{wind-sea}}$  is only related to local wind forcing, the changes with TS are more  
167 localized and well defined, with increasing left-right asymmetry as TS grows. In the center of  
168 the cyclone,  $H_s^{\text{wind-sea}}$  values are negative (i.e. below average) for all TS. This is the reason for the  
169 low values found for  $H_s$ . In contrast to  $H_s^{\text{wind-sea}}$ ,  $H_s^{\text{swell}}$  (Figure 2, bottom row) displays lower  
170 values where winds are stronger (rear-right sector) and higher at the cyclone center.  $H_s^{\text{swell}}$   
171 increases with larger TS. For fast moving cyclones (TS >10 m/s) maxima extend towards the  
172 tail of the structure. It is worth noting that  $H_s^{\text{swell}}$  is directed towards the center of the cyclone in  
173 those areas where values are higher.

174           The edge of the cyclone derived from the atmospheric fields (green circles) does not  
175 always match its imprint in the pattern of  $H_s$ . Actually, the center defined by the wave field  
176 shows a downward shift, with this displacement being larger for faster cyclones. This effect is  
177 especially evident for  $H_s^{\text{wind-sea}}$ , which can be explained by the more smoothed downscaled wind  
178 fields as mentioned above.

## 179           **4.2 Strength of cyclones**

180           The cyclone intensity has been defined on the basis of the maximum [wind speed](#) ( $S_{\text{max}}$ )  
181 observed. Again three ranges [of maximum wind speed](#) have been explored, namely  $S_{\text{max}}$ -smaller  
182 than 6 m/s, between 6 and 9 m/s and larger than 9 m/s. The resulting composites are mapped in  
183 Figure 3 for  $H_s$  and its components  $H_s^{\text{wind-sea}}$  and  $H_s^{\text{swell}}$ , showing that the impact of the intensity  
184 is very strong for all wave parameters. For the weakest cyclones, maximum  $H_s$  is only 0.2 m  
185 while it reaches 1.8 m for the most intense (Figure 3, upper row). Higher  $H_s$  and  $H_s^{\text{wind-sea}}$  are  
186 found in all cases at the rear-right sector, where winds are stronger. Interestingly, unlike for  
187 faster cyclones, in this case stronger cyclones follow the wind patterns more closely (see for  
188 example the center of  $H_s^{\text{wind-sea}}$  without any displacement).

189           On the other hand, the wave age is dependent upon the cyclone intensity, since it is  
190 inversely proportional to  $S$ . Therefore, the same classification has been used to build the WA  
191 composites (Figure S2). Those areas in Figure S2 in which the uncertainty in WA is of the same  
192 order as its value have been shadowed in gray to avoid misinterpretations. The smallest values  
193 of WA are found in the rear-right sector where [wind speeds](#) is higher. As expected, the WA  
194 decreases with more intense cyclones, and simultaneously the left right symmetry is enhanced.  
195 The center of the cyclone is the region where WA reaches its maximum, indicating that it  
196 corresponds to an area of swell predominance. This is in agreement with the findings in Figure  
197 3.

### 198           **4.3 Size of cyclones**

199           Composites of  $H_s$  have been built for three different cyclone radii: smaller than 500 km,  
200 between 500 and 600 km and above 600 km. The results, displayed in Figure 4, indicate that the  
201 largest cyclones show stronger winds and therefore higher  $H_s$  (Figure 4, upper row). These  
202 fields thus allow linking the cyclone size to its intensity, a relationship that will be further  
203 explored in the next section. Values of  $H_s$  are around 0.6 m for the smallest cases and reach 1.6  
204 m for the largest cyclones. The same applies to  $H_s^{\text{wind-sea}}$  (middle row), whereas  $H_s^{\text{swell}}$  also  
205 increases at the center of the cyclone for the largest events. In fact, the largest cyclones show a  
206 wave pattern more consistent with the expected winds in terms of their spatial structure and the  
207 coincidence of their centers.

### 208           **Discussion and concluding remarks**

209           To our knowledge, this is the first time that this type of analysis has been applied in a  
210 marginal sea for extra-tropical cyclones, whose strength is within the same range that the much  
211 more studied tropical storms (15-30 m/s). Hence, our results are complementary to earlier works  
212 aimed at describing the wave climate under the influence of TCs, which are more intense

213 perturbations that develop in large basins and with different spatial footprints on surface waves  
214 (e.g. Timmermans *et al.*, 2017).

215 Our findings point out that under the influence of cyclones,  $H_s$  anomalies as well as  
216  $H_s^{\text{wind-sea}}$  and  $H_s^{\text{swell}}$  anomalies, significantly increase when these events are more intense, as  
217 expected. However, these changes are far from homogeneous; as cyclone velocity adds up to  
218 local wind on the right side of the cyclone, it has a stronger impact on wind speed in this sector,  
219 and therefore it is where the highest  $H_s$  and  $H_s^{\text{wind-sea}}$  are found. This effect is more intense and  
220 localized with larger TS and, in particular, there is an increase in the left-right asymmetry and a  
221 backward displacement of the center defined by waves direction from the theoretical cyclone  
222 center (Figure 2). We have found that the highest waves are located in the rear-right sector of the  
223 cyclone, where winds are stronger (Figure 2). This result contrasts with earlier assessments in  
224 which the front-right quadrant has been identified as the area of maximum wave height (Wright  
225 *et al.*, 2001; Moon *et al.*, 2004; Doyle *et al.*, 2012). However, all these cases focused on TCs.  
226 Most studies show that in the case of the hurricanes the largest waves are located in the front-  
227 right sector, being linked to the swell generated by the TC that become trapped within the  
228 cyclone due to a resonance effect occurring when the perturbation travels at a speed close to the  
229 wave propagation speed (see Moon *et al.* (2003) for a detailed explanation of this dynamic  
230 fetch). In the case of hurricanes, this swell can be even larger than the locally generated waves.  
231 Conversely, in the Western Mediterranean this resonance effect cannot be developed due to the  
232 small size of the basin with respect to the size of the cyclones: the average radius of the  
233 cyclones we are considering is 551 km whereas in our study the center of the furthest cyclone is  
234 only 238 km from the closest shoreline. On the other hand, a recent study of Hwang and Walsh  
235 (2016) using synthetic aperture radar (SAR) measurements of wave parameters under TCs  
236 identified the rear-right region as the one with more intense air-sea exchange of energy and  
237 momentum by using empirical fetch growth functions (see Figures 10 and 11 therein). Winds

238 over 35 m/s may stop wave growth, which will occur specially in the rear-right quadrant where  
239 both wind is stronger and air-sea exchange more efficient. This wave breaking at an earlier stage  
240 will be accompanied by whitecaps on the ocean surface (Hwang and Walsh, 2016). In this study  
241 the absence of the trapping resonance effect and of hurricane force winds, suggests that, in  
242 agreement with our results, higher waves develop on the rear right side. The enhancement of the  
243 left-right asymmetry reported above is also found for cyclones with increasing radii, which are  
244 more powerful than small ones. Nevertheless, we cannot establish a robust statistical  
245 relationship between TS and R on the basis of our data set due to the limitations in the  
246 determination of TS, as will be further discussed below.

247 The separation of total significant wave height into its  $H_s^{\text{wind-sea}}$  and  $H_s^{\text{swell}}$  components  
248 has revealed that the effects of increasing cyclone intensity are opposed. With stronger cyclones  
249  $H_s^{\text{wind-sea}}$  increases in the right-rear quadrant and decreases in the cyclone center, whereas  $H_s^{\text{swell}}$   
250 drops down in the right-rear sector and reaches its maximum at the center, although with values  
251 up to three times smaller than the  $H_s^{\text{wind-sea}}$ . Wave directions of the swell component in Figures 2,  
252 3 and 4 confirm that these waves were generated in the rear-right sector and moved towards the  
253 center. The overall picture of the combination of the two components is consistent with the WA  
254 results (Figure S2), with higher values in the cyclone center that identify the swell component.  
255 For the sake of completeness, we have also repeated the composites for the fetch (not shown)  
256 that led to the same conclusion: fetch increases along with swell propagation, from the rear-right  
257 quadrant towards the cyclone center.

258 This swell propagation is, again, hardly comparable with what happens with TCs  
259 because of the relative small dimensions and the topographic complexity of the Western  
260 Mediterranean Sea.  $H_s^{\text{wind-sea}}$  under TCs radiates out of the maximum wind speed zone (right side  
261 of a cyclone moving upwards). For instance, in the case of hurricane Bonnie, swell was

262 observed roughly aligned in with the cyclone track and outside the cyclone (Wright *et al.*, 2001;  
263 Holthuijsen *et al.*, 2012).

264 In addition to the spatial patterns of the waves generated by the cyclones, it is also  
265 interesting to investigate the relationship between the maximum Hs reached in each event,  $H_s^{\max}$ ,  
266 and the cyclones characteristics (TS, intensity and radii). In our data set we found that  $H_s^{\max}$  is  
267 not correlated to TS, despite faster cyclones are associated with more intense events and thus  
268 with stronger winds. Yet, we conclude that this apparent contradiction is due to the way we have  
269 estimated TS, a methodology that is clearly limited by the spatial resolution ( $1.125^\circ \approx 125$  km)  
270 of the cyclone data set (Campins *et al.*, 2011). For example, one cyclone during two consecutive  
271 time steps (separated 6 hours to each other) can apparently remain stationary at the same  
272 location and, at the third time step 6 hours later, suddenly jump to a neighboring grid point; in  
273 this case the estimated velocities between two consecutive time steps can differ from the real  
274 velocity because the cyclone has moved continuously.

275 On the other hand, according to the Figures 3 and 4,  $H_s^{\max}$  is related to the cyclone radii  
276 and maximum wind intensity (the correlation coefficients R are 0.40 and 0.93, respectively).  
277 Figure 5 represents the scatter points of  $H_s^{\max}$  and the maximum wind speed  $S_{\max}$  for each  
278 cyclone. The curve that best fits both variables, [among a set of polynomials of different order](#),  
279 is given by:

$$280 \quad H_s^{\max} = 0.01S_{\max}^2 + 0.165S_{\max} - 0.211 \quad (1)$$

281 [Where  \$S\_{\max}\$  represents the maximum wind speed.](#) Adding the cyclone radius to this relationship  
282 does not improve the fitting (the correlation coefficient increases by 0.005 at the best), because  
283 the radius and the maximum winds are correlated to each other. As expected,  $H_s^{\max}$  is highly  
284 dependent on [the maximum wind speed](#) because the transfer of energy from the atmosphere

285 to the sea is higher. In addition,  $H_s^{\max}$  corresponds to a large extent to wind-sea since these  
286 waves are locally dominant over swell in all our case studies.

287         Despite some limitations in the cyclones database such as the spatial coarse resolution  
288 or the assumption that cyclones are perfect circles, this study demonstrates a clear and spatially  
289 heterogeneous imprint of cyclones on wave patterns. This pattern, predicting the highest waves  
290 in the rear-right sector, differs from that observed in the much more investigated cases with TCs.  
291 And so do the potentially hazardous impacts of these phenomena. Thus, depending on the  
292 location and the direction of propagation of the cyclone, the area where the highest waves will  
293 be developed can be easily forecasted. Moreover, the relationship between maximum  $H_s$  and  
294 maximum wind speed permits the estimation of the size of these waves parameterized with the  
295 atmospheric characteristics of the event, which can be relevant for coastal protection. In  
296 principle, a cyclone climatology in which the intensity, size, direction and TS of each event is  
297 accurately computed, could serve to identify the coastal sectors that are more exposed to the  
298 high waves generated by the cyclones. With the present climatology for the Western  
299 Mediterranean basin though, the assessment of coastal vulnerability is hampered by the low  
300 spatial resolution and difficulty to estimate the TS with enough precision. Yet, we anticipate that  
301 a higher resolution data set could have utility for such practical purposes and would allow to  
302 focus especially on the most intense episodes.

### 303 **Acknowledgments**

304 This work was partially supported by the Research Project CLIMPACT (CGL201454246-C21-  
305 R, AEI/FEDER, UE) funded by the Spanish Ministry of Economy. T. Toomey is grateful to the  
306 Région Bretagne JALI supporting grant. J.M. Sayol is hired under the NWO-VIDI grant number  
307 397 864.13.011. J.M. Sayol thanks Prof. Leo Oey for organizing the Princeton Journal Club, an  
308 inspiration for this work. G. Jordà acknowledges a Ramón y Cajal contract (RYC-2013-14714)

309 funded by the Spanish Ministry of Economy and the Regional Government of the Balearic  
310 Islands  
311

312 **References**

313

314 Besio G., R. Briganti, A. Romano, L. Mentaschi, and P. De Girolamo (2017), Time clustering of  
315 wave storms in the mediterranean sea, *Natural Hazards and Earth System Sciences*, 17(3),  
316 505–514, doi:10.5194/nhess-17-505-2017.

317 Campins J., A. Genovés, M. A. Picornell, and A. Jansà (2011), Climatology of mediterranean  
318 cyclones using the era-40 dataset, *International Journal of Climatology*, 31(11), 1596–  
319 1614, doi:10.1002/joc.2183.

320 Cardone V. J., R. E. Jensen, D. T. Resio, V. R. Swail, and A. T. Cox (1996), Evaluation of  
321 contemporary ocean wave models in rare extreme events: The halloween storm of october  
322 1991 and the storm of the century of march 1993, *Journal of Atmospheric and Oceanic*  
323 *Technology*, 13(1), 198–230,  
324 doi: 10.1175/1520-0426(1996)013<0198:EOCOWM>2.0.CO;2

325 Cline I. M. (1920), Relation of changes in storm tides on the coast of the gulf of mexico to the  
326 center and movement of hurricanes, *Monthly Weather Review*, 48(3), 127–146,  
327 doi:10.1175/1520-0493(1920)48<127:ROCI&T>2.0.CO;2.

328 da Rocha R. P., S. Sugahara, and R. B. da Silveira (2004), Sea waves generated by extratropical  
329 cyclones in the south atlantic ocean: Hindcast and validation against altimeter data,  
330 *Weather and Forecasting*, 19(2), 398–410,  
331 doi:10.1175/1520-0434(2004)019<0398:SWGBEC>2.0.CO;2.

332 Dacre H. F., M. K. Hawcroft, M. A. Stringer, and K. I. Hodges (2012), An extratropical cyclone  
333 atlas: A tool for illustrating cyclone structure and evolution characteristics, *Bulletin of the*  
334 *American Meteorological Society*, 93(10), 1497–1502, doi:10.1175/BAMS-D-11- 00164.1.

335 [Déqué, M. and J.P. Piedelievre; \(1995\). High resolution climate simulation over Europe, \*Cimate\*  
336 \*Dynamics\*, 11 \(1995\), pp. 321-339](#)

337 [M. Déqué, M., C. Devreton, A. Braun, D. Cariolle \(1994\) The Arpege/Ifs atmosphere model – a  
338 contribution to the French community climate modelling, \*Climate Dynamics\*, 10-\(4-5\)  
339 \(1994\), pp. 249-266](#)

340 [Déqué, M. \(2007\) Frequency of precipitation and temperature extremes over France in an  
341 anthropogenic scenario: Model results and statistical correction according to observed  
342 values, \*Global and Planetary Change, Volume 57, Issues 1–2, Pages 16-26\*](#)

343

344 De Zolt S., P. Lionello, A. Nuhu, and A. Tomasin (2006), The disastrous storm of 4 november  
345 1966 italy, *Natural Hazards and Earth System Sciences*, 6(5), 861–879,  
346 doi:10.5194/nhess-6-861-2006.

347 Doyle J., P. Black, C. Amerault, S. Chen, and S. Wang (2012), Wind-wave interaction under  
348 hurricane conditions: a decade of progress, in *Proceedings of ECMWF Workshop on*  
349 *Ocean Waves, 25-27 June*, edited by ECMWF.

29

30



- 350 Fan Y., I. Ginis, T. Hara, C. W. Wright, and E. J. Walsh (2009), Numerical simulations and  
 351 observations of surface wave fields under an extreme tropical cyclone, *Journal of Physical*  
 352 *Oceanography*, 39(9), 2097–2116, doi:10.1175/2009JPO4224.1.
- 353 Guimarães P. V., L. Farina, and E. E. Toldo Jr. (2014), Analysis of extreme wave events on the  
 354 southern coast of Brazil, *Natural Hazards and Earth System Sciences*, 14(12), 3195– 3205,  
 355 doi:10.5194/nhess-14-3195-2014.
- 356 Harley M. D., I. L. Turner, M. A. Kinsela, J. H. Middleton, P. J. Mumford, K. D. Splinter, M. S.  
 357 Phillips, J. A. Simmons, D. J. Hanslow, and A. D. Short (2017), Extreme coastal erosion  
 358 enhanced by anomalous extratropical storm wave direction, *Scientific Reports*, 7(1), 6033,  
 359 doi:10.1038/s41598-017-05792-1.
- 360 Holthuijsen L. H., M. D. Powell, and J. D. Pietrzak (2012), Wind and waves in extreme  
 361 hurricanes, *Journal of Geophysical Research: Oceans*, 117(C9), n/a–n/a,  
 362 doi:10.1029/2012JC007983, c09003.
- 363 Hwang P. A., and E. J. Walsh (2016), Azimuthal and radial variation of windgenerated surface  
 364 waves inside tropical cyclones, *Journal of Physical Oceanography*, 46(9), 2605–2621,  
 365 doi:10.1175/JPO-D-16-0051.1.
- 366 Innocentini V., and E. D. S. C. Neto (1996), A case study of the 9 August 1988 South Atlantic  
 367 storm: numerical simulations of the wave activity, *Weather and Forecasting*, 11(1), 78– 88,  
 368 doi:10.1175/1520-0434(1996)011<0078:ACSOTA>2.0.CO;2.
- 369 Jansà A. (1997), A general view about mediterranean meteorology: cyclones and hazardous  
 370 weather, *INM/WMO International Symposium on cyclones and hazardous weather in the*  
 371 *Mediterranean, Palma de Mallorca.*
- 372 Jordà G., D. Gomis, E. Alvarez Fanjul, and S. Somot (2012), Atmospheric contribution to  
 373 Mediterranean and nearby Atlantic sea level variability under different climate change  
 374 scenarios, *Global and Planetary Change*, 80-81, 198–214,  
 375 doi:https://doi.org/10.1016/j.gloplacha.2011.10.013.
- 376 Lionello P., P. Malanotte-Rizzoli, and R. Boscolo (2006), *Mediterranean Climate Variability*,  
 377 438 pp., Elsevier.
- 378 Lionello P., I. F. Trigo, V. Gil, M. L. R. Liberato, K. M. Nissen, J. G. Pinto, C. C. Raible, M.  
 379 Reale, A. Tanzarella, R. M. Trigo, S. Ulbrich, and U. Ulbrich (2016), Objective  
 380 climatology of cyclones in the Mediterranean region: a consensus view among methods  
 381 with different system identification and tracking criteria, *Tellus A: Dynamic Meteorology*  
 382 *and Oceanography*, 68(1), 29,391, doi:10.3402/tellusa.v68.29391.
- 383 Maheras P., H. Flocas, I. Patrikas, and C. Anagnostopoulou (2001), A 40-year objective  
 384 climatology of surface cyclones in the Mediterranean region: spatial and temporal  
 385 distribution, *International Journal of Climatology*, 21(1), 109–130, doi:10.1002/joc.599.
- 386 Martínez-Asensio A., M. Marcos, G. Jordà, and D. Gomis (2013), Calibration of a new wind-  
 387 wave hindcast in the Western Mediterranean, *Journal of Marine Systems*, 121-122  
 388 (Supplement C), 1 – 10, doi:<https://doi.org/10.1016/j.jmarsys.2013.04.006>.

- 389 Moon I.-J., I. Ginis, T. Hara, H. L. Tolman, C. W. Wright, and E. J. Walsh (2003), Numerical  
390 simulation of sea surface directional wave spectra under hurricane wind forcing, *Journal*  
391 *of Physical Oceanography*, 33(8), 1680–1706, doi:10.1175/2410.1.
- 392 Moon I.-J., I. Ginis, and T. Hara (2004), Effect of surface waves on airsea momentum exchange.  
393 part II: Behavior of drag coefficient under tropical cyclones, *Journal of the Atmospheric*  
394 *Sciences*, 61(19), 2334–2348,  
395 doi:10.1175/1520-0469(2004)061<2334:EOSWOA>2.0.CO;2
- 396 Nissen K. M., G. C. Leckebusch, J. G. Pinto, D. Renggli, S. Ulbrich, and U. Ulbrich (2010),  
397 Cyclones causing wind storms in the mediterranean: characteristics, trends and links to  
398 large- scale patterns, *Natural Hazards and Earth System Sciences*, 10(7), 1379– 1391,  
399 doi:10.5194/nhess-10-1379-2010.
- 400 Picornell M., A. Jans`a, A. Genov`es, and J. Campins (2001), Automated database of  
401 mesocyclones from the HIRLAM(INM)-0.5° analyses in the western Mediterranean,  
402 *International Journal of Climatology*, 21(3), 335–354, doi:10.1002/joc.621.
- 403 [Rudeva, I., and S.K. Gulev \(2007\) Climatology of cyclone size characteristics and their changes](#)  
404 [during the cyclone life cycle,; Monthly Weather Review, 135, pp. 2568- 2587, doi:](#)  
405 [10.1175/MWR3420.1](#)
- 406 Sartini L., F. Cassola, and G. Besio (2015), Extreme waves seasonality analysis: an application  
407 in the Mediterranean Sea, *Journal of Geophysical Research: Oceans*, 120 (9), 6266– 6288,  
408 doi:10.1002/2015JC011061.
- 409 Stephens S. A., and D. Ramsay (2014), Extreme cyclone wave climate in the Southwest Pacific  
410 Ocean: Influence of the El Niño Southern Oscillation and projected climate change,  
411 *Global and Planetary Change*, 123(Part A), 13 – 26,  
412 doi:<https://doi.org/10.1016/j.gloplacha.2014.10.002>.
- 413 Tannehill I. R. (1936), Sea swells in relation to movement and intensity of tropical storms,  
414 *Monthly Weather Review*, 64(7), 231–238,  
415 doi:10.1175/1520-0493(1936)64<231b:SSIRTM>2.0.CO;2.
- 416 The Wamdi Group (1988), The WAM Model-A Third Generation Ocean Wave Prediction  
417 Model, *Journal of Physical Oceanography*, 18(12), 1775–1810, doi:10.1175/1520-  
418 0485(1988)018<1775:TWMTGO>2.0.CO;2.
- 419 Timmermans B., D. Stone, M. Wehner, and H. Krishnan (2017), Impact of tropical cyclones on  
420 modeled extreme wind-wave climate, *Geophysical Research Letters*, 44(3), 1393–1401,  
421 doi:10.1002/2016GL071681, 2016GL071681.
- 422 Trigo I. F., T. D. Davies, and G. R. Bigg (1999), Objective climatology of cyclones in the  
423 mediterranean region, *Journal of Climate*, 12(6), 1685–1696, doi:10.1175/1520-  
424 0493(2002)130<0549:COCMIT>2.0.CO;2.
- 425 Trigo I. F., G. R. Bigg, and T. D. Davies (2002), Climatology of Cyclogenesis Mechanisms in  
426 the Mediterranean, *Monthly Weather Review*, 130(3), 549–569, doi:10.1175/1520-  
427 0493(2002)130<0549:COCMIT>2.0.CO;2.

428 Wright C. W., E. J. Walsh, D. Vandemark, W. B. Krabill, A. W. Garcia, S. H. Houston, M. D.  
429 Powell, P. G. Black, and F. D. Marks (2001), Hurricane directional wave spectrum spatial  
430 variation in the open ocean, *Journal of Physical Oceanography*, 31(8), 2472–2488,  
431 doi:10.1175/1520-0485(2001)031<2472:HDWSSV>2.0.CO;2..  
432

433 **Figure captions**

434  
435 Figure 1. Spatial distribution of  $H_s$  over the Western Mediterranean for the same cyclone at four  
436 different time steps. Black arrows represent the wind field and the cyclone is plotted as a green  
437 circle.

438 Figure 2. Spatial distribution of  $H_s$ ,  $H_s^{\text{wind-sea}}$ , and  $H_s^{\text{swell}}$  for a TS of 5 m/s or less (left), between 5  
439 and 10 m/s (center) and 10 m/s or more (right). Black arrows represent waves mean direction,  
440 dark purple contours represent the ME (order of  $10^{-1}$  m here) while white contours show zones  
441 of maximum wind speed anomalies. N indicates the number of observations used.

442 | Figure 3. Spatial distribution of  $H_s$ ,  $H_s^{\text{wind-sea}}$ , and  $H_s^{\text{swell}}$  for a [S<sub>max</sub>-maximum wind speed \(S<sub>max</sub>\)](#) of  
443 6 m/s or less (left), between 6 and 9 m/s (center) and 9 m/s or more (right). Black arrows  
444 represent waves mean direction, dark purple contours represent the ME (order of  $10^{-1}$  m here)  
445 while white contours show zones of maximum wind speed anomalies. N indicates the number of  
446 observations used.

447 Figure 4. Comparison of total  $H_s$ ,  $H_s^{\text{wind-sea}}$ , and  $H_s^{\text{swell}}$  for cyclones with radius of 0-500 km (left),  
448 500-600 km (center), or 600 km and more (right). Black arrows represent waves mean direction,  
449 dark purple contours represent the ME (order of  $10^{-1}$  m here) while white contours show zones  
450 of maximum wind speed anomalies. N indicates the number of observations used.

451 | Figure 5. Scatter plot of  $H_s^{\text{max}}$  as a function of [the maximum wind speed \(S<sub>max</sub>\)](#). The solid line  
452 represent the equation modeling the relation between  $H_s^{\text{max}}$  and [the maximum wind speed S<sub>max</sub>](#).  
453 Dashed lines represent  $H_s^{\text{max}}$  at 99.5% prediction interval. Computed from a sample of 5178  
454 observations (df+3), the determination coefficient is 0.863 ( $R^2$ ).

455

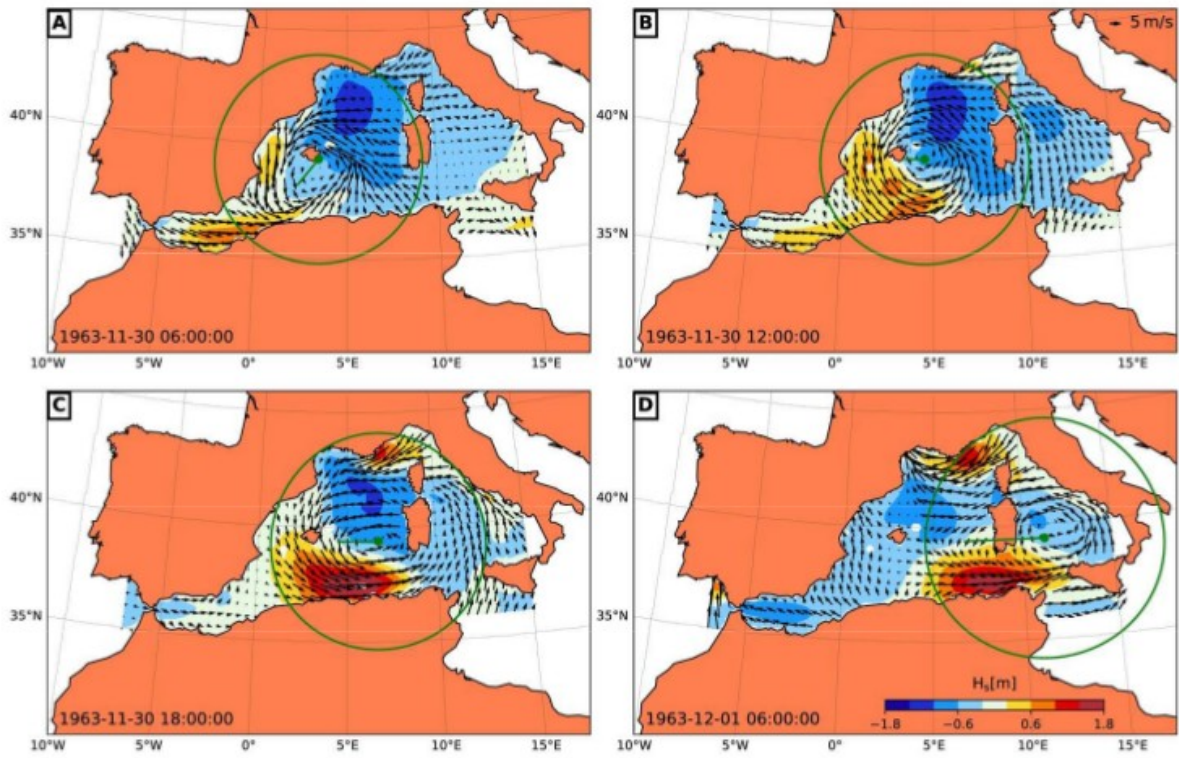


Figure 1: Spatial distribution of  $H_s$  over the Western Mediterranean for the same cyclone at four different time steps. Black arrows represent the wind field and the cyclone is plotted as a green circle.



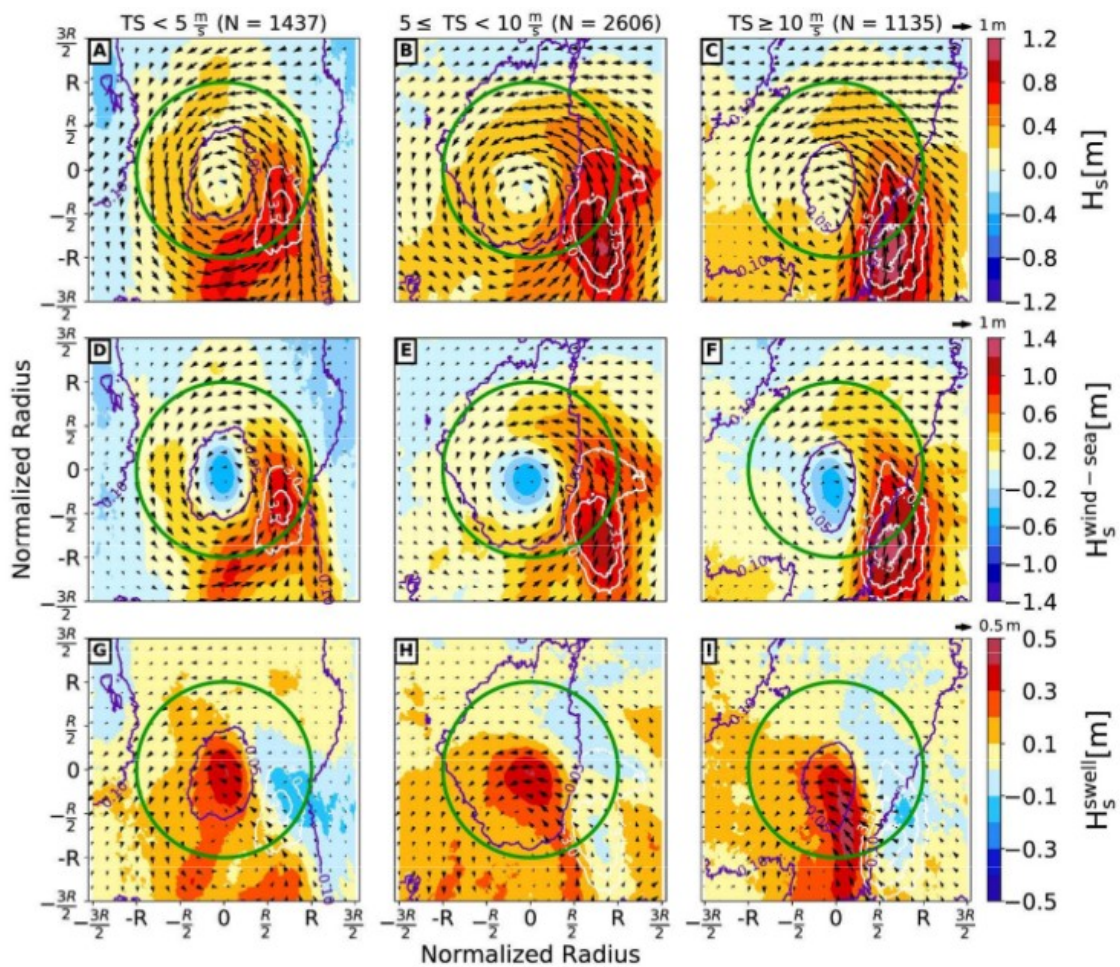


Figure 2: Spatial distribution of  $H_s$ ,  $H_s^{\text{wind-sea}}$ , and  $H_s^{\text{swell}}$  for a TS of 5 m/s or less (left), between 5 and 10 m/s (center) and 10 m/s or more (right). Black arrows represent waves mean direction, dark purple contours represent the ME (order of  $10^{-1}$  m here) while white contours show zones of maximum wind speed anomalies. N indicates the number of observations used.

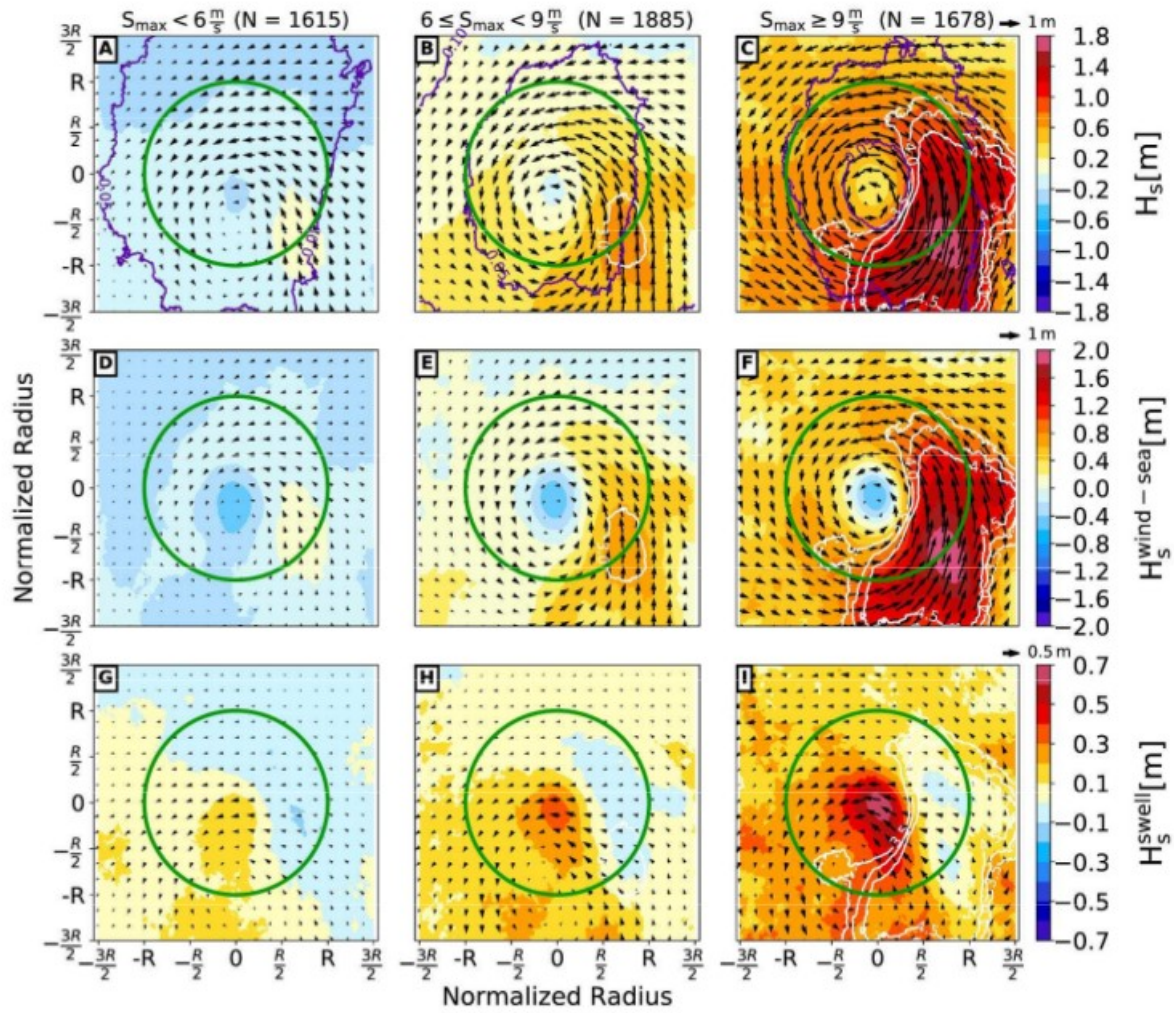


Figure 3: Spatial distribution of  $H_s$ ,  $H_s^{\text{wind-sea}}$ , and  $H_s^{\text{swell}}$  for a maximum wind speed ( $S_{\max}$ ) of 6 m/s or less (left), between 6 and 9 m/s (center) and 9 m/s or more (right). Black arrows represent waves mean direction, dark purple contours represent the ME (order of  $10^{-1}$  m here) while white contours show zones of maximum wind speed anomalies. N indicates the number of observations used.



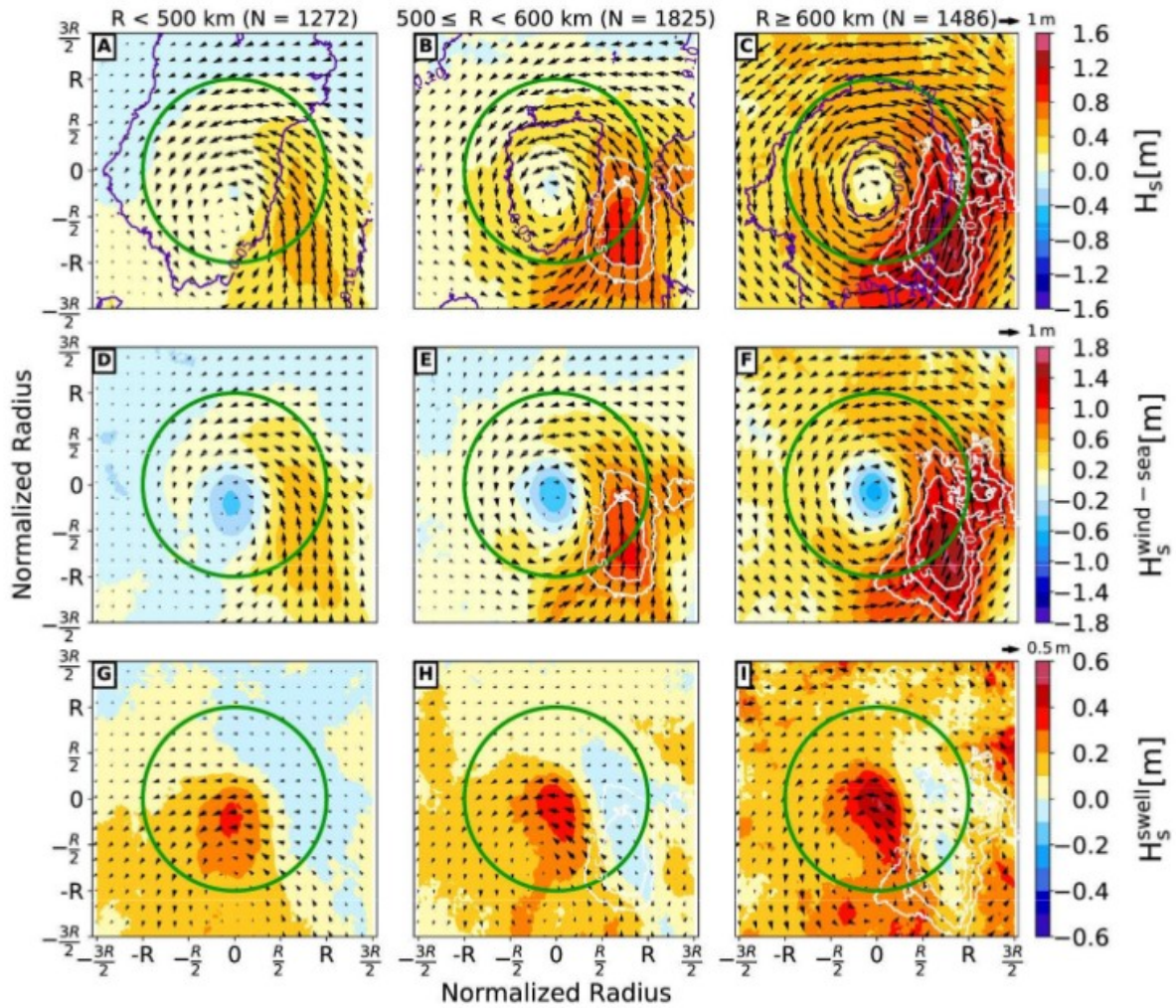


Figure 4: Comparison of total  $H_s$ ,  $H_s^{\text{wind-sea}}$ , and  $H_s^{\text{swell}}$  for cyclones with radius of 0-500 km (left), 500-600 km (center), or 600 km and more (right). Black arrows represent waves mean direction, dark purple contours represent the ME (order of  $10^{-1}$  m here) while white contours show zones of maximum wind speed anomalies. N indicates the number of observations used.



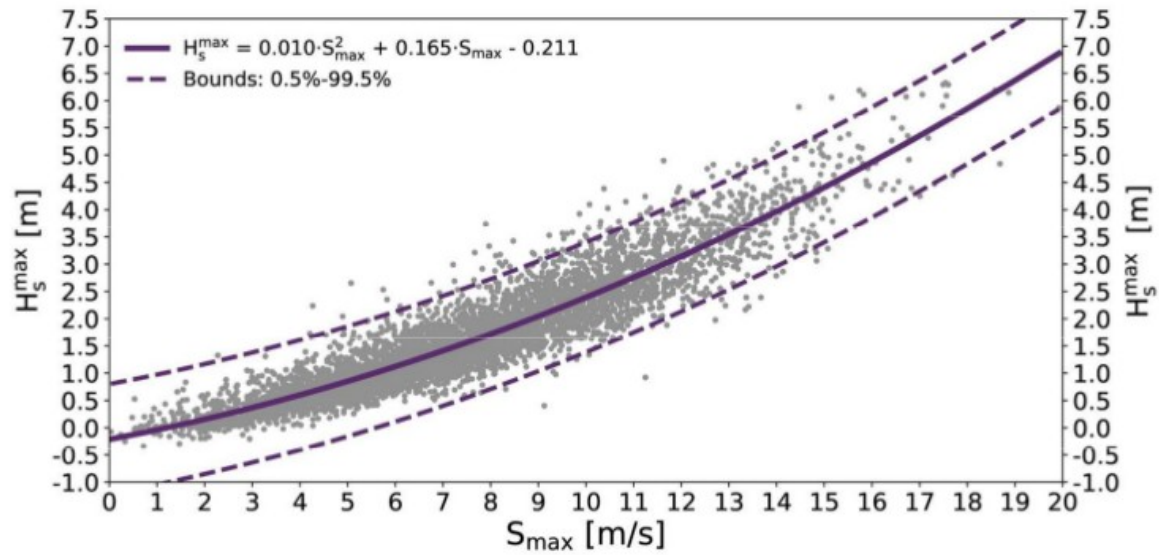


Figure 5: Scatter plot of  $H_s^{\max}$  as a function of the maximum wind speed ( $S_{\max}$ ). The solid line represent the equation modeling the relation between  $H_s^{\max}$  and maximum wind speed. Dashed lines represent  $H_s^{\max}$  at 99.5% prediction interval. Computed from a sample of 5178 observations ( $df+3$ ), the determination coefficient is 0.863 ( $R^2$ ).